Phase Matching in Lower Dimensions

H. Tamura, H. Nguyen, P. R. Berman, and A. Kuzmich
Department of Physics, University of Michigan, Ann Arbor, Michigan 48109, USA

(Received 31 March 2020; accepted 10 September 2020; published 13 October 2020)

Phase matching refers to a process in which atom-field interactions lead to the creation of an output field that propagates coherently through the interaction volume. By studying light scattering from arrays of cold atoms, we show that conditions for phase matching change as the dimensionality of the system decreases. In particular, for a single atomic chain, there is phase-matched reflective scattering in a cone about the symmetry axis of the array that scales as the square of the number of atoms in the chain. For two chains of atoms, the phase-matched reflective scattering can be enhanced or diminished as a result of Bragg scattering. Such scattering can be used for mapping collective states within an array of neutral atoms onto propagating light fields and for establishing quantum links between separated arrays.

DOI: 10.1103/PhysRevLett.125.163601

Beginning with the pioneering demonstrations of second-harmonic generation [1,2] and photon echoes [3], phase matching has played a critical role in nonlinear and quantum optics. When N atoms are excited in free space, collective emission can result in a number of ways, some of which are discussed by Dicke [4] in his seminal paper. One type of collective emission, which we refer to as superradiance, is produced when two-level atoms are prepared in a completely inverted or phase-matched initial state in an ensemble for which the so-called cooperativity parameter is greater than or of order unity. A second type of collective emission, on which we focus here, is simply phase-matched emission from an array of noninteracting atoms, that is, a limiting case where the field radiated by a given atom has a negligible effect on the dynamics of the other atoms. This is the type of interference effect typically encountered in optical coherent transients [5]. Yet a third type of collective emission is somewhat of a hybrid of the first two. Atoms are prepared in a collective, phased single-excitation state using a single-photon pulse [6–8]. The atoms do not acquire a dipole moment, but the emission pattern can mirror that of phase-matched emission. In this and related schemes in which the dimensions of the excitation volume are large compared with the wavelength of the excitation field(s), the $\mathbf{k}$ vector of the phase-matched emission satisfies a momentum conservation condition involving the $\mathbf{k}$ vectors of the excitation fields. For example, in a four-wave mixing process with incident field $\mathbf{k}$ vectors $\mathbf{k}_1$, $\mathbf{k}_2$, and $\mathbf{k}_3$, a possible phase-matched outgoing field propagates in the $\mathbf{k}_s = \mathbf{k}_1 - \mathbf{k}_2 + \mathbf{k}_3$ direction. The signal results from an average over the distribution of positions of individual atomic emitters and does not require a specific spatial arrangement of the atoms in the sample, in contrast to Bragg scattering.

In an experimental situation involving a *single* cw excitation field incident on a low density atomic vapor, collective scattering still occurs, but its signature is very different from that in the four-wave mixing experiment. The collectively scattered light is phase matched only in the direction of the input field and it interferes with the incident light to diminish the incident field's intensity. In order to get constructive interference in other directions, a specific atomic array is needed, rather than a disordered vapor. This type of collective emission is nothing more than Bragg scattering and it has been demonstrated using chains of trapped ions [9–11], two-dimensional Mott insulators [12], and ensembles of atoms in 1D and 3D lattices [13,14]. In Bragg scattering, it is necessary to localize each emitter to well within the wavelength of the incident radiation. Deviations from perfect localization wash out any constructive interference and reduce the fidelity of associated quantum protocols.

Diverse applications of quantum information require interconnected quantum nodes that are capable of local processing and error correction. Integration of local processing and memory enhances performance of quantum repeaters over lossy channels, enables distributed quantum processing and sensing, and allows for entanglement resources to be shared within the network. In prior work with a single atomic qubit per node, entanglement between an atomic qubit and a photon [15–18] and entanglement between remote atomic qubits [19–21] have been realized. High-fidelity one-qubit gates [22,23] and pairwise entanglement of neighboring and next-to-nearest neighbor sites [24,25] in 1D and 2D arrays have also been demonstrated. However, the integration of communication and processing capabilities remains an outstanding challenge. High-quality interference for light emitted from a reconfigurable array of trapped neutral atoms is essential for using such arrays in a way that combines processing and mapping between atomic and photonic states [26].

In this Letter, we propose and demonstrate noncollinear phase-matching geometries that have suppressed sensitivity

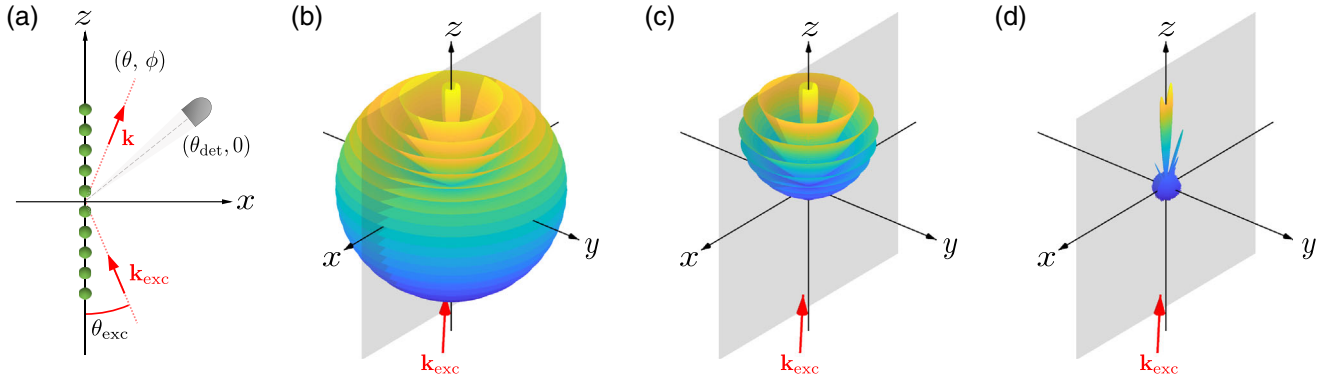

FIG. 1. Bragg scattering from a one-dimensional atomic chain. (a) A linear chain with $N = 10$ atoms separated by $d = 7.49$ μm is aligned along the z axis. An excitation laser with wave vector $\mathbf{k}_{\mathrm{exc}}$ is directed onto the chain at an angle $\theta_{\mathrm{exc}} = 4°$ with respect to the z axis. The scattered light with wave vector $\mathbf{k}$ is detected as a function of spherical angles (θ, ϕ). (b) Structure factor $S(\theta, \phi)$ for equal separation of atoms, and (c) in the presence of disorder of atomic positions with standard deviations $(\sigma_x, \sigma_y, \sigma_z) = (0, 0, 0.3\lambda)$, and (d) $(\sigma_x, \sigma_y, \sigma_z) = (0.3\lambda, 2.4\lambda, 0.3\lambda)$. Gray panels represent the x-z plane in which the excitation laser propagates. To measure the scattered signal, we use a detector whose axis has polar angles $(\theta_{\mathrm{det}}, 0)$.

to particle localization. In the first geometry, there is a single atomic chain whose axis makes a small angle θ_{exc} with the propagation vector of the incident field [Fig. 1(a)]. In the second geometry, two atomic chains are used to observe interference fringes having near-unity visibility. The ability to obtain high-quality phase-matched scattering from an array of individually controllable atoms represents an important step toward the realization of scalable atom-photon interfaces.

The central idea for achieving this goal is the observation that, as the dimensionality of the system decreases, new directions for phase matching appear even for a disordered atomic array. The origin of this effect can be understood by considering a structure factor $S(\theta, \phi) = \sum_{j,j'=1}^{N} e^{-i\Phi_{jj'}}$ for scattering of off-resonant radiation from independent atoms. The scattered intensity is proportional to S, with

$$\Phi_{jj'} = kX_{jj'}(\sin\theta\cos\phi + \sin\theta_{\mathrm{exc}}) + kY_{jj'}\sin\theta\sin\phi + kZ_{jj'}(\cos\theta - \cos\theta_{\mathrm{exc}}),$$

being an overall phase for the scattering, $\mathbf{k}_{\mathrm{exc}} = k(-\sin\theta_{\mathrm{exc}}\hat{\mathbf{x}} + \cos\theta_{\mathrm{exc}}\hat{\mathbf{z}})$ the incident field propagation vector, (θ, ϕ) polar and azimuthal scattering angles, $\mathbf{R}_j = X_j\hat{\mathbf{x}} + Y_j\hat{\mathbf{y}} + Z_j\hat{\mathbf{z}}$ the position vector for atom j, and $\mathbf{R}_{jj'} = \mathbf{R}_j - \mathbf{R}_{j'}$. For phase matching from a disordered atomic array, the phase $\Phi_{jj'}$ must vanish for *all* $\mathbf{R}_{jj'}$. In three dimensions, phase matching is possible only in the direction of the incident field $(\theta = \theta_{\mathrm{exc}}, \phi = \pi)$. However, if the atoms are confined to the $y - z$ plane, there is perfect *reflective* phase matching in the plane of incidence provided $\theta = \theta_{\mathrm{exc}}$ and $\phi = 0$. If the dimensionality is further reduced to a chain of atoms along the z axis, there is phase matching in a *cone* with polar angle θ_{exc}. Deviations from perfect phase matching arising from excursions out of the plane or chain can be reduced by taking $\theta_{\mathrm{exc}} \ll 1$.

We first consider an ideal situation in which N atoms are confined to a one-dimensional chain in the z direction with fixed spacing d between the atoms. In this limit, as illustrated in Fig. 1(b) for our experimental parameters ($d \approx 7.49$ μm, $\lambda \approx 780.24$ nm, $\theta_{\mathrm{exc}} \approx 4°$), there is constructive conical collective scattering for several values of θ satisfying the Bragg condition. In our experiment, the confinement and separation of the trapped atoms is somewhat disordered, owing to imperfect positioning of the traps, finite atomic temperature, and random filling of trap sites. When effects of atom position deviations along the z axis are included, the number of Bragg scattering cones diminishes, Fig. 1(c). Nonzero values of X_j and Y_j further restrict the emission pattern to a single cone about the symmetry axis having maxima at $\phi = 0$, $\phi = \pi$, Fig. 1(d) and Supplemental Material [27].

We use cold ^{87}Rb atoms confined in an array formed by holographic optical microtraps. Once N atoms are prepared in an array containing N_t traps, we image these atoms to determine the number of traps that are filled. We then apply a magnetic field of $B \approx 2.0$ G along the excitation laser axis and employ a gated probing-cooling sequence. During this sequence, the excitation laser and cooling beams are switched on and off in an alternating manner with durations of 0.9 ms and 2.2 ms, respectively. The scattered light is detected with an avalanche photodiode (APD) gated on only during the excitation period. The excitation laser, propagating along the magnetic field, is σ^+ polarized and red detuned by $\delta/(2\pi) \approx 62$ MHz from the $|g\rangle = |5S_{1/2}, F = 2, m_F = 2\rangle \leftrightarrow |e\rangle = |5P_{3/2}, F' = 3, m_{F'} = 3\rangle$ transition. The beam waist of the excitation laser is $\sim$0.1 mm. The scattered light is collected by an achromatic doublets lens with focal length $f = 150$ mm and coupled into a single-mode fiber directed toward the APD. The detector axis has polar angles $(\theta_{\mathrm{det}}, 0)$, see Fig. 1(a). The detection mode has a waist of $\approx$13.3 μm. After a total of

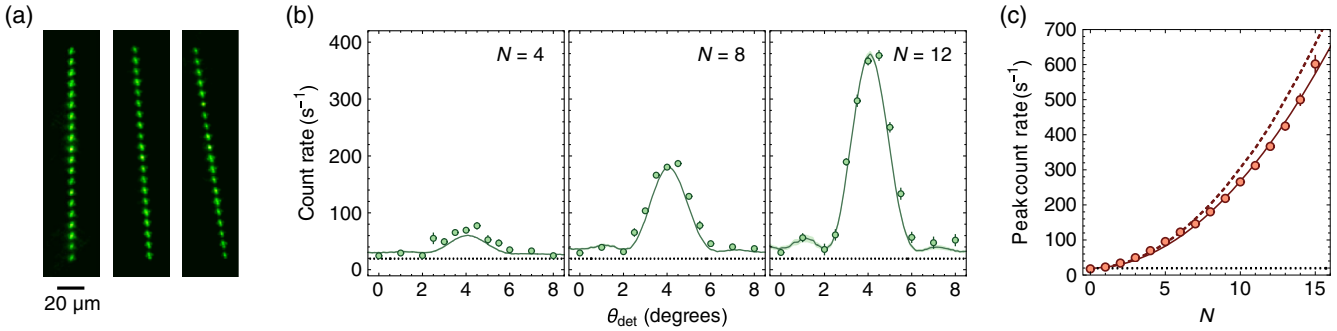

FIG. 2. Phase-matched emission from a single chain. (a) Averaged atomic fluorescence images of a linear chain containing $N_t = 20$ traps. The left image shows a configuration in which the atoms are aligned along with the detection mode axis, i.e., $\theta_{det} = 0°$. For the middle (right) image, the chain is prepared such that $\theta_{det} \approx 4°(8°)$. (b) The measured photocount rate as a function of θ_{det} for $N = 4$, 8, 12. Each point is an average of randomly filled chains with a given N. Error bars represent one standard deviation of the observed photoelectric counting events. The green lines are the numerical results based on a Monte Carlo simulation with 1000 runs. The shading on the line represents the standard deviation of the simulation divided by the square root of the averaged number of trials in the experiments. (c) The peak count rate as a function of N. Each point and its error bar represent the observed value at $\theta_{det} = \theta_0 = 4°$. For the single-shot measurement of $N = 15$, we associate a $\sqrt{M}$ Poissonian error for M photoelectric count events. The solid (dashed) line represents the numerical simulation with (without) displacement of atomic positions due to imperfect positioning of the traps and finite temperature effects. The black dotted lines in (b),(c) show the detection background measured without loading atoms.

1200 cycles of the gated probing-cooling sequence with repetition rate of ≈300 Hz, an additional imaging of the traps is taken to determine the final number of atoms N_f in the array. For the data analysis, only experimental samples with $N_f = N$ are postselected to remove atom loss effects. We repeat this entire sequence in determining a photon count rate averaged over atomic configurations in the array for a given N.

In the first geometry, we use a linear chain with $N_t = 20$ traps separated by $d \approx 7.49$ μm. To experimentally find a reflective phase-matching condition, both θ_{det} and θ_{exc} are varied by rotating the chain axis with $\theta_0 = (\theta_{det} + \theta_{exc})/2$ kept fixed at ≈4°. Figure 2(a) displays averaged fluorescence images of the chain for three different θ_{det}. For $\theta_{det} = 0°$ (left image) the chain is oriented along the detection mode, while for $\theta_{det} = 2\theta_0 \approx 8°$ (right image) the chain is aligned along the axis of the excitation field. Reflective phase matching is expected to appear when $\theta_{det} = \theta_0 \approx 4°$ (middle image). The measured photon count rates as a function of θ_{det} for various N are shown in Fig. 2(b), where the horizontal axis is zeroed within the calibration error of ±0.11°. We observe an enhanced photon count rate, attributed to the reflective phase-matched emission, for each N at around the expected value of θ_{det}.

The experimental data are offset from the background signal [represented by the black dotted lines in Fig. 2(b)]. The origin of this offset can be traced to (1) deviations from perfect periodicity of the trap potentials, (2) temperature effects, (3) random filling of the traps, and (4) inelastic scattering of the incident field [32].

For our experimental conditions, the theoretical expression for the scattered light intensity in steady state can be written as

$$I(\mathbf{r}) \propto |\mathbf{F}_{sc}(\mathbf{r})|^2 \left(\sum_j^N \rho_{ee}^{(j)} + \sum_{j \neq j'}^N \rho_{ge}^{(j)} \rho_{eg}^{(j')} e^{-i\Phi_{jj'}} \right), \quad (1)$$

where $\mathbf{F}_{sc}$ is a σ^+ dipole radiation field amplitude, $\rho_{ee}^{(j)}$ is an excited state population, and $\rho_{ge}^{(j)}$ denotes the single atom coherence between $|g\rangle$ and $|e\rangle$. Both $\rho_{ee}^{(j)}$ and $\rho_{ge}^{(j)}$ are obtained as a function of the Rabi frequency Ω and detuning δ from the solution of the steady-state optical Bloch equations. We do not measure the intensity *per se*, rather we measure the absolute square of the scattered field *amplitude* projected onto the detection mode (see Supplemental Material [27]). To include the effects of disorder, we compute a signal averaged over different atomic configurations. For N atoms and N_t traps, a specific configuration is obtained by placing each atom at random in the traps, with at most one atom in each trap. The displacement of atomic positions originates from imperfect positioning of the traps and from the finite temperature T. In these simulations Ω and θ_0 are taken to be free parameters to fit the data for $2 \leq N \leq 15$. We obtain $\Omega/(2\pi) = 3.24(4)$ MHz and $\theta_0 = 4.19(2)°$ without the calibration error. The results of the numerical simulations, displayed as solid lines in Fig. 2(b), successfully reproduce the entire shape of the observed signal.

Under conditions of phase matching, the relative phase $\Phi_{jj'}$ is insensitive to position disorder along the y and z axes, that is $\partial\Phi_{jj'}/\partial Y_{jj'} = \partial\Phi_{jj'}/\partial Z_{jj'} = 0$. Therefore, random filling of the traps by the atoms does not affect the peak signal. However, there is a small sensitivity of the peak signal to displacements along the x axis, since $\partial\Phi_{jj'}/\partial X_{jj'} = 2k \sin\theta_0 \equiv q_x$. Therefore, even for fully coherent scattering, averaging of the peak signal with a Boltzmann distribution of positions in the

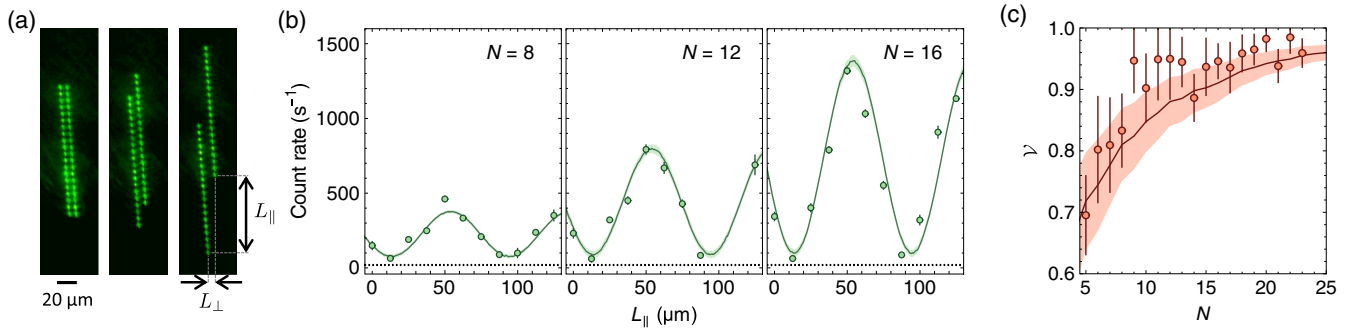

FIG. 3. Observation of constructive and destructive Bragg scattering from two chains. (a) Averaged fluorescence images of two linear chains under three different values of the chain separation $L = L_\parallel \sin\theta_0 + L_\perp \cos\theta_0$. (b) Measured photon count rate as a function of $L_\parallel$ for $N = 8$, 12, 16. Error bars represent one standard deviation for M photoelectric counting events. The green lines are the numerical simulation based on a Monte Carlo simulation with 1000 runs. The shading on the line represents the standard deviation of the simulation divided by the square root of the averaged number of trials in the experiments. The black dotted lines show the detection background which is measured without loading atoms. (c) The observed scaling of the interference visibilities $\mathcal{V}$ as a function of the total number of atoms N. Each point is obtained by fitting the observed fringe by a sinusoidal function. Error bars indicate the fitting errors with 68% confidence intervals. The solid line is the result of the numerical simulation together with the standard error of the mean (shaded area).

x direction reduces the structure factor from N^2 to $f_{\mathrm{DW}}N^2 + (1 - f_{\mathrm{DW}})N$, where f_{DW} is a Debye-Waller factor [33] given by $\langle e^{-i\Phi_{jj'}}\rangle \approx e^{-q_x^2\sigma_x^2}$ and $\langle\cdots\rangle$ denotes the average over the Boltzmann distributions. In Fig. 2(c) the observed peak count rate (red points) is displayed together with a theoretical curve for an equally spaced chain without any position disorder (dashed line). The fact that the curves almost overlap is consistent with the Debye-Waller factor of $f_{\mathrm{DW}} \approx 0.93$. The maximum scattered intensity is also diminished by an N independent factor of about 10% resulting from the projection onto the detector mode.

In the second geometry, we extend the system to two chains, each composed of $N_t/2 = 20$ equally spaced traps. The chain axes are chosen to satisfy the reflective phase-matched condition $\theta_{\mathrm{det}} = \theta_{\mathrm{exc}} = \theta_0$ measured in the first geometry. The two chains are separated by a distance $L_\perp$ in the direction orthogonal to the detection axis that is chosen equal to the spacing d between the adjacent traps [left image in Fig. 3(a)]. To observe interference of reflective phase-matched emission from the two chains, each chain is displaced by $L_\parallel/2$ in the direction away from each other along the detection axis [middle and right images in Fig. 3(a)]. Therefore, the shortest distance between the two chains can be written by $L = L_\parallel \sin\theta_0 + L_\perp \cos\theta_0$.

Figure 3(b) displays the measured photon count rates as a function of the chain separation $L_\parallel$ for $N = 8, 12$, and 16. These results show constructive and destructive Bragg scattering, and they are analyzed using sinusoidal fits. These interference fringes provide information about geometrical parameters of the experimental setup. According to Bragg's law: $2L\sin\theta_0 = m\lambda$, the expected interference period is $\Delta L_\parallel = \lambda/(2\sin^2\theta_0)$ and mth order constructive emission appears at $L_\parallel^{(m)} = m\Delta L_\parallel - L_\perp \cot\theta_0$. Taking into account the observed period and second order peak position $(\Delta L_\parallel, L_\parallel^{(2)}) = [10.56(5), 6.92(2)]d$ averaged over $5 \le N \le 23$, we obtain $d = 7.49(11)$ μm and $\theta_0 = 4.01(4)°$. The solid lines in Fig. 3(b) are the results of the numerical simulations with the obtained values of d, θ_0.

In Fig. 3(c) we show the measured interference visibility $\mathcal{V} = (I_{\mathrm{max}} - I_{\mathrm{min}})/(I_{\mathrm{max}} + I_{\mathrm{min}})$ as a function of the total number of atoms N. When averaged over the range $20 \le N \le 23$, the background-subtracted $\mathcal{V}$ we obtain is 0.97(2), significantly higher than that reported in prior studies of multiatom Bragg scattering [9–14]. The clear reduction in visibility for smaller numbers of atoms N is due mostly to an increased imbalance in the atom number between the two chains. It can be understood as follows: for constructive interference, the relative phase $\Phi_{jj'}$ is zero for any two atoms in the same chain and a multiple of 2π for any two atoms in different chains. Therefore the maximum fringe intensity I_{max} is insensitive to an imbalance in the number of atoms between the individual chains and scales as $\sim N^2$. On the other hand, for *complete* destructive interference, the relative phase between atoms in different chains must be an odd multiple of π *and* the number of atoms in each chain must be the same. For unequal numbers of atoms in the two chains, destructive interference cannot be complete. The solid line in Fig. 3(c) is based on our numerical simulations which include random filling of traps, inelastic scattering, and atomic position disorder, see Supplemental Material [27].

It is well known that restricting the dimensionality of a quantum system can radically alter its global properties, as well as interparticle interactions and, in doing so, allow for new applications that do not occur in higher dimensions. Frequently in such settings, many-body effects play a critical role. In contrast, our work demonstrates that the reduced dimensionality of a quantum system can be

important in a situation with no strong interparticle correlations. Specifically, we have demonstrated phase-matched coherent scattering for one- and two-dimensional geometries of a single-atom qubit array suitable for storage and processing of quantum information. High-visibility interference fringes are observed for two atomic chains as a function of their separation. Atom arrays connected to photonic channels can provide a technology foundation for future quantum networks with efficient multipartite scaling. Networks using such arrays as quantum nodes would offer a variety of schemes to encode, transfer, and manipulate quantum information within and between the nodes of the network for distributed quantum computation, communication, and sensing [26]. A logical extension of this work could involve the creation of multiatom entangled states in a setting where the atoms can be individually addressed and their various combinations chosen for entangled state generation.

This work was supported by the Army Research Laboratory (ARL) Center for Distributed Quantum Information, Air Force Office of Scientific Research, and the National Science Foundation.

[1] P. A. Franken, A. E. Hill, C. W. Peters, and G. Weinreich, Generation of Optical Harmonics, Phys. Rev. Lett. **7**, 118 (1961).
[2] P. D. Maker, R. W. Terhune, M. Nisenoff, and C. M. Savage, Effects of Dispersion and Focusing on the Production of Optical Harmonics, Phys. Rev. Lett. **8**, 21 (1962).
[3] N. A. Kurnit, I. D. Abella, and S. R. Hartmann, Observation of a Photon Echo, Phys. Rev. Lett. **13**, 567 (1964).
[4] R. H. Dicke, Coherence in spontaneous radiation processes, Phys. Rev. **93**, 99 (1954).
[5] P. R. Berman and V. S. Malinovsky, *Principles of Laser Spectroscopy and Quantum Optics* (Princeton University Press, Princeton, 2011).
[6] L.-M. Duan, M. D. Lukin, J. I. Cirac, and P. Zoller, Long-distance quantum communication with atomic ensembles and linear optics, Nature (London) **414**, 413 (2001).
[7] T. Chanelière, D. N. Matsukevich, S. D. Jenkins, S.-Y. Lan, T. A. B. Kennedy, and A. Kuzmich, Storage and retrieval of single photons transmitted between remote quantum memories, Nature (London) **438**, 833 (2005).
[8] M. O. Scully, E. S. Fry, C. H. R. Ooi, and K. Wódkiewicz, Directed Spontaneous Emission from an Extended Ensemble of *N* Atoms: Timing is Everything, Phys. Rev. Lett. **96**, 010501 (2006); P. R. Berman and J.-L. Le Gouët, Phase-matched emission from an optically thin medium following one-photon pulse excitation: Energy considerations, Phys. Rev. A **83**, 035804 (2011).
[9] U. Eichmann, J. C. Bergquist, J. J. Bollinger, J. M. Gilligan, W. M. Itano, D. J. Wineland, and M. G. Raizen, Young's Interference Experiment with Light Scattered from Two Atoms, Phys. Rev. Lett. **70**, 2359 (1993).
[10] S. Wolf, J. Wechs, J. von Zanthier, and F. Schmidt-Kaler, Visibility of Young's Interference Fringes: Scattered Light from Small Ion Crystals, Phys. Rev. Lett. **116**, 183002 (2016).
[11] P. Obšil, A. Lešundák, T. Pham, G. Araneda, M. Čížek, O. Číp, R. Filip, and L. Slodička, Multipath interference from large trapped ion chains, New J. Phys. **21**, 093039 (2019).
[12] C. Weitenberg, P. Schauß, T. Fukuhara, M. Cheneau, M. Endres, I. Bloch, and S. Kuhr, Coherent Light Scattering from a Two-Dimensional Mott Insulator, Phys. Rev. Lett. **106**, 215301 (2011).
[13] G. Birkl, M. Gatzke, I. H. Deutsch, S. L. Rolston, and W. D. Phillips, Bragg Scattering from Atoms in Optical Lattices, Phys. Rev. Lett. **75**, 2823 (1995).
[14] S. Slama, C. von Cube, A. Ludewig, M. Kohler, C. Zimmermann, and Ph. W. Courteille, Dimensional crossover in Bragg scattering from an optical lattice, Phys. Rev. A **72**, 031402(R) (2005).
[15] D. N. Matsukevich and A. Kuzmich, Quantum state transfer between matter and light, Science **306**, 663 (2004).
[16] B. B. Blinov, D. L. Moehring, L.-M. Duan, and C. Monroe, Observation of entanglement between a single trapped atom and a single photon, Nature (London) **428**, 153 (2004).
[17] J. Volz, M. Weber, D. Schlenk, W. Rosenfeld, J. Vrana, K. Saucke, C. Kurtsiefer, and H. Weinfurter, Observation of Entanglement of a Single Photon with a Trapped Atom, Phys. Rev. Lett. **96**, 030404 (2006).
[18] L. Li, Y. O. Dudin, and A. Kuzmich, Entanglement between light and an optical atomic excitation, Nature (London) **498**, 466 (2013).
[19] D. N. Matsukevich, T. Chanelière, S. D. Jenkins, S.-Y. Lan, T. A. B. Kennedy, and A. Kuzmich, Entanglement of Remote Atomic Qubits, Phys. Rev. Lett. **96**, 030405 (2006).
[20] D. L. Moehring, P. Maunz, S. Olmschenk, K. C. Younge, D. N. Matsukevich, L.-M. Duan, and C. Monroe, Entanglement of single-atom quantum bits at a distance, Nature (London) **449**, 68 (2007).
[21] J. Hofmann, M. Krug, N. Ortegel, L. Gérard, M. Weber, W. Rosenfeld, and H. Weinfurter, Heralded entanglement between widely separated atoms, Science **337**, 72 (2012).
[22] T. Xia, M. Lichtman, K. Maller, A. W. Carr, M. J. Piotrowicz, L. Isenhower, and M. Saffman, Randomized Benchmarking of Single-Qubit Gates in a 2D Array of Neutral-Atom Qubits, Phys. Rev. Lett. **114**, 100503 (2015).
[23] Y. Wang, A. Kumar, T.-Y. Wu, and D. S. Weiss, Single-qubit gates based on targeted phase shifts in a 3D neutral atom array, Science **352**, 1562 (2016).
[24] H. Levine, A. Keesling, G. Semeghini, A. Omran, T. T. Wang, S. Ebadi, H. Bernien, M. Greiner, V. Vuletić, H. Pichler, and M. D. Lukin, Parallel Implementation of High-Fidelity Multiqubit Gates with Neutral Atoms, Phys. Rev. Lett. **123**, 170503 (2019).
[25] T. M. Graham, M. Kwon, B. Grinkemeyer, Z. Marra, X. Jiang, M. T. Lichtman, Y. Sun, M. Ebert, and M. Saffman, Rydberg-Mediated Entanglement in a Two-Dimensional Neutral Atom Qubit Array, Phys. Rev. Lett. **123**, 230501 (2019).
[26] C. Monroe, R. Raussendorf, A. Ruthven, K. R. Brown, P. Maunz, L.-M. Duan, and J. Kim, Large-scale modular quantum-computer architecture with atomic memory and photonic interconnects, Phys. Rev. A **89**, 022317 (2014).

[27] See Supplemental Material at http://link.aps.org/supplemental/10.1103/PhysRevLett.125.163601 for more experimental and theory details, which includes Refs. [28–31].
[28] N. Schlosser, G. Reymond, and P. Grangier, Collisional Blockade in Microscopic Optical Dipole Traps, Phys. Rev. Lett. **89**, 023005 (2002).
[29] C. Tuchendler, A. M. Lance, A. Browaeys, Y. R. P. Sortais, and P. Grangier, Energy distribution and cooling of a single atom in an optical tweezer, Phys. Rev. A **78**, 033425 (2008).
[30] Y. R. P. Sortais, H. Marion, C. Tuchendler, A. M. Lance, M. Lamare, P. Fournet, C. Armellin, R. Mercier, G. Messin, A. Browaeys, and P. Grangier, Diffraction-limited optics for single-atom manipulation, Phys. Rev. A **75**, 013406 (2007).
[31] A. Rojo (private communication).
[32] B. R. Mollow, Power spectrum of light scattered by two-level systems, Phys. Rev. **188**, 1969 (1969).
[33] W. M. Itano, J. C. Bergquist, J. J. Bollinger, D. J. Wineland, U. Eichmann, and M. G. Raizen, Complementarity and Young's interference fringes from two atoms, Phys. Rev. A **57**, 4176 (1998).